Materials Today Chemistry 38 (2024) 102046

Contents lists available at ScienceDirect

Materials Today Chemistry

journal homepage: www.journals.elsevier.com/materials-today-chemistry/

pH-dependent catalytic activity of Au and Pd-based hybrid cryogels by investigating the acid/base nature of the polymeric phase

Stefano Scurti [a], Giuseppe Proietto Salanitri [a,c], Tommaso Mecca [d], Elena Rodríguez-Aguado [e], Juan Antonio Cecilia [e], Giusy Curcuruto [c], Sabrina Carola Carroccio [c], Daniele Caretti [a], Nikolaos Dimitratos [a,b,*]

[a] Industrial Chemistry "Toso Montanari" Department, University of Bologna, Viale Risorgimento 4, 40136, Bologna, Italy
[b] Center for Chemical Catalysis-C3, Alma Mater Studiorum Università di Bologna, Viale Risorgimento 4, 40136, Bologna, Italy
[c] Institute for Polymers, Composites and Biomaterials (IPCB) – CNR, Via Paolo Gaifami 18, 95126, Catania, Italy
[d] Institute for Biomolecular Chemistry (ICB) – CNR, Via Paolo Gaifami 18, 95126, Catania, Italy
[e] Departamento de Química Inorgánica, Cristalografía y Mineralogía (Unidad Asociada al ICP-CSIC), Facultad de Ciencias, Universidad de Málaga, Campus de Teatinos, 29071, Málaga, Spain

ARTICLE INFO

Keywords:
Hybrid nanomaterials
Cryogels
pH dependence reaction
Catalytic reaction mechanism

ABSTRACT

Over the last decade, cryogels have proven to be effective catalytic supports in various hybrid systems for the conversion of 4-nitrophenol (4-NP) to 4-aminophenol (4-NP). A critical determinant influencing the conversion of nitroaromatic compounds in the presence of sodium borohydride is the solution pH as suggested from Grzeschik's model. This study aims to investigate the catalytic mechanism and the role of pH in reactions mediated by hybrid catalysts. In particular, polymeric cryogels with different acid/base properties were prepared and used as supports for the *in-situ* preparation of Au and Pd nanocatalysts. Notably, catalytic tests showed the significant influence of the polymeric support's acidity on 4-NP reduction, with poly(acrylic acid)-based catalysts emerging as the most effective systems. To further probe the reaction mechanism, a series of catalytic tests were carried out, and the results demonstrated the effect of pH on the reaction process, allowing to propose a novel mechanism based on an extension of Grzeschik's model. Moreover, data emphasized the pivotal role of the polymer in the catalytic mechanism, showcasing its capacity to tune catalytic activity by altering the acid/base properties of the matrix substrates.

1. Introduction

Several research endeavours have been directed towards the development of more efficient methodologies for fabricating metal nanoparticles characterized by controlled shapes, sizes, low polydispersity, high purity, and robust stability in designated dispersion media. The research has particularly focused on achieving the synthesis of monodispersed nanoparticles by the utilization of polymers due to an enhanced comprehension of the underlying stabilization processes. The outcomes have emphasized a compelling correlation between the resultant materials' properties—such as stability and surface chemistry—and the specific attributes of the employed polymers [1–7]. Moreover, coating metal nanoparticles with polymeric ligands significantly influences their interactions with catalyzed substances, impacting catalytic performance in terms of activity, stability, and product yield. The crucial role of protective ligands covering the nanoparticles is evident, affecting reactant accessibility and acting as a dynamic shell that modulates both activity and selectivity [8–13]. In this view, it is imperative to meticulously document and analyze how the characteristics of the polymer ligand, encompassing factors such as molecular weight and functional groups, can exert a direct influence not only on the topological features of nanomaterials but also on the related catalytic activity of metal-polymer systems. The same properties can be translated into preparing hybrid nano-catalysts, where an active phase is closely in contact with polymeric counterparts, enhancing the effects associated with the polymeric matrix. Furthermore, the use of supported colloidal nanocatalysts on gel-like architectures (e.g., hydrogels, xerogels, or cryogels) represents a suitable strategy to produce a novel class of materials where the chemical flexibility of the organic phase can be combined with their thermo-mechanical properties and the potential for

* Corresponding author. Industrial Chemistry "Toso Montanari" Department, University of Bologna, Viale Risorgimento 4, 40136, Bologna, Italy.
E-mail address: nikolaos.dimitratos@unibo.it (N. Dimitratos).

https://doi.org/10.1016/j.mtchem.2024.102046
Received 19 January 2024; Received in revised form 5 April 2024; Accepted 8 April 2024
Available online 12 April 2024

recovery, aligning with the principles of environmental sustainability [14–16]. An example was represented in the Gu et al. work where they reported a Pd-loaded porphyrin-based porous organic polymer containing bifunctional catalytic sites, which was used to catalyse the tandem C–H arylation and Suzuki coupling reactions [17]. Kudaibergenov described catalytic reactors based on metal nanoparticles (Au and Pd) immobilized within the pores of nano-, micro-, and macro-sized acrylic-based polymeric gels and in the surface or hollow of polymeric membranes [18,19]. Xiang and collaborators have developed adsorbent resorcinol-formaldehyde-thiourea (RFT) resin to recover Au(III) and, at the same time, reduce it in metal form with possible applications in catalytic fields [20]. The employment of these type of polymeric networks are strictly related to their porosity that represented a crucial parameter for catalytic applications.

Among them, polymeric macroporous network obtained via cryogelation methods are becoming very attractive for environmental and energy application [21–24]. Due to the appealing use of cryogels as catalytic supports, in the last decade several hybrid systems have been successfully tested to convert 4-NP to the aminophenol in batch or in continuous flow set-up [15,25,26]. While the catalytic mechanism of this reaction remains under investigation, a critical parameter influencing the conversion of nitroaromatic compounds in the presence of sodium borohydride mediated by nanostructured catalysts is the solution pH [27–31]. In this regard, Grzeschik and colleagues conducted a computational study combined with an experimental kinetic approach [32]. They demonstrated how the dissociation of $NaBH_4$ is influenced by the pH value of the solution and therefore its effect in 4-NP reduction in the presence of colloidal metal nanoparticles. Building upon Grzeschik's model, this study primarily aims to conduct a systematic investigation, extending the proposed mechanism to hybrid catalysts through the preparation of polymeric cryogels with varying acidity. These cryogels serve as supports in the preparation of Au and Pd nanocatalysts. The materials synthesized were subsequently tested in the hydrogenation of 4-nitrophenol. The intention herein, is to explore the reaction mechanism and the contribution of the polymeric phase in catalysis demonstrating how a specific catalyst design, considering the impact of the polymeric counterpart, represents a viable strategy for selectively tuning catalytic activity.

2. Experimental part

2.1. Materials

Tetrachloroauric acid trihydrate ($HAuCl_4{\cdot}3H_2O$), potassium hexachloropalladate (K_2PdCl_6), sodium borohydride ($NaBH_4$), 4-nitrophenol (4NP), 2-hydroxyethyl methacrylate (HEMA), methacrylic acid (MAA), N,N,N′,N′-tetramethylethylenediamine (TMEDA), ammonium persulfate (APS), N,N′-methylenebis(acrylamide) (MBAA) are commercially available chemicals and were used without further purification process, except AEMA.

2-aminoethyl methacrylate (AEMA) was purified by extraction with ethyl acetate, to remove the polymerization inhibitor (phenothiazine) since imparted a blue colour to the final material. The solvents were used without further purification processes.

2.2. Cryogels preparation

Three different acrylic-based polymeric cryogels were synthesized by solution radical cryo-copolymerization using APS-TMEDA as an initiator system and MBAA as a water-soluble crosslinker. All cryogels were synthesized using a 10 % w/w monomer and crosslinker aqueous solution with a monomer/MBAA molar ratio of 6:1 and an amount of APS-TMEDA of 1 % w/w for the preparation of *p*-HEMA and *p*-AEMA, while for the synthesis of *p*-MAA cryogels is 2 % w/w. The percentages used were referred to the amount of monomer employed for each synthesis.

In the case of *p*-MAA and *p*-AEMA, before the addition of APS and TMEDA, the solution containing the monomers was neutralized with NaOH 0.1 M.

The polymerization mixtures were stirred for about 1 min and then transferred into two pre-cooled plastic syringes at 0 °C. The syringes were placed in a cryostat at −15 °C for about 24 h. At the end of the cryopolymerization, samples were thawed at room temperature and washed several times with a mixture of H_2O/EtOH/diethyl ether, increasing progressively the concentration of the less volatile solvent. The purified cryogels were dried first under a nitrogen flow, then with a vacuum pump, and finally in a vacuum oven [33,34]. The polymerization yields were in the range from 80 to 90 %.

2.3. Preparation of hybrid nanomaterials

The deposition of gold and palladium nanoparticles in polymeric cryogels was performed by wet-impregnation approach. A defined amount of dry cryogel was put in contact with a water solution of the metal precursor ($HAuCl_4$ or K_2PdCl_6) to have a metal loading of 1 % w/w. During the impregnation phase, polymer swelling was observed, allowing the complete absorption of the metal solution. Subsequently, a freshly prepared $NaBH_4$ solution with a molar ratio of 5:1 compared to the metal was added to reduce the metal cations absorbed into the polymer matrix. Adding the reducing agent, a rapid colour change was observed: from white to red or grey, related to gold and palladium nanoparticles formation respectively. The obtained hybrid nanomaterials were washed following the same procedure employed for the bare cryogel purification to favour the solubilization of the by-products deriving from the impregnation phase (e.g. borides and chlorides). The samples were labelled as "name of polymer_metal"(e.g., *p*-MAA_Au).

2.4. Characterization

The bare and hybrid cryogels were characterized by several spectroscopic, thermal and microscopic analyses. All samples were characterized by Fourier Transform Infrared Spectroscopy (FT-IR), acquiring the spectra through an ATR-IR Bruker Alpha I spectrometer. The macroporous morphology of the polymeric cryogel pre- and post-impregnation, as well as porous size distribution, were investigated by Scanning Electron Microscopy (SEM) Zeiss Supra 25 field emission microscope equipped with an EDX probe. Data were acquired and processed using Phenom Porometric 1.1.2.0 software (Phenom-World BV, Eindhoven, Netherlands). The thermal stability of cryogels was studied by thermogravimetric analysis (TGA) using a TA Instruments Q500 apparatus. The analyses were conducted in a nitrogen atmosphere (flow rate 60 mL/min) with a heating ramp of 10 °C/min, from 25 °C to 800 °C. To verify the complete absorption of the active phase, the supernatant solution not absorbed in the impregnation step was analyzed by microwave plasma atomic emission spectroscopy (MP-AES) using an Agilent 4210 MP-AES Atomic Emission Spectrometer. The presence of zero-valent metal nanoparticles was verified using PHI Versa Probe II X-ray photoelectron spectrometer (XPS) using a monochromatic Al Kα radiation (52.8 W, 15 kV, 1486.6 eV) and a dual beam charge neutralizer. The X-ray photoelectron spectra obtained were analyzed using PHI SmartSoft software and processed using the MultiPak 9.6.0.15 package. The surface charge of polymeric cryogels was measured by zeta potential analysis as a function of pH using a Malvern Panalytical (Malvern, United Kingdom) Zetasizer Nano ZS instrument. The titrations were carried out with an Ag/AgCl glass electrode. The instrument was calibrated by two buffer solutions: potassium phosphate (pH = 7) and potassium hydrogen phthalate (pH = 4). The catalytic tests in function of the pH were conducted using a XS model PC 8+ DHS pHmeter equipped with a thermocouple. The measures were carried out with a glass electrode Amel 211/SGG/12 with a pH accuracy of 0.01 calibrated with standard solutions at specific pH values (4.01 and 7). Transmission electron microscopy (TEM) images were obtained by FEI Tecnai G2

Spirit TWIN 120 kV TEM operating at a 120 kV acceleration voltage and the images were processed by using the ImageJ to determine average particle size and particle size distribution.

Swelling tests were performed on dried bare cryogels. After water uptake and removal of its surplus from the surface, mass measurements were carried out. The total uptake for all samples was determined by calculating the increase of cumulative mass at fixed time intervals. The equilibrium swelling degree was measured by weighting the wet sample immersed in water for 30 min. Conversely, the adsorption kinetic was estimated after keeping the samples in contact with a slight excess of water for selected times, followed by quick removal of the excess of unabsorbed water.

The adsorbed water was evaluated by weighting the sample in the function of time and normalizing all data. The equilibrium swelling degree can be calculated using the following formula:

$$Swelling\ degree\ \% : \frac{(m_w - m_d)}{m_d} \bullet 100$$

where m_w is the weight of the wet cryogel, and m_d is the weight of the dry cryogel.

2.5. Catalytic test

Before initiating the catalytic tests, the hybrid nanocatalysts were milled to achieve a finely homogeneous powder with a diameter ranging between 0.2 and 0.4 mm. Initially, the samples were subjected to contact with a liquid nitrogen bath and then ground in a mortar to facilitate milling. The resulting powder underwent sieving, and the fraction with a diameter of 0.3 mm was recovered.

2.5.1. Nitrophenol calibration

UV–visible spectroscopic analyses were performed in a 1 cm path length cuvette using an *in-situ* Agilent Cary 3500 UV–Vis Spectrometer. The extinction coefficient was determined by using five solutions of different 4-NP concentrations ($1.5{\cdot}10^{-4}$ M, $1.0{\cdot}10^{-4}$ M, $5.0{\cdot}10^{-5}$ M, $2.5{\cdot}10^{-5}$ M, $1.0{\cdot}10^{-5}$ M), and $4.5{\cdot}10^{-3}$ M in $NaBH_4$. The calibration curve was plotted, giving an extinction coefficient of 18,400 $M^{-1}cm^{-1}$, close to the literature value of 18,000 $M^{-1}cm^{-1}$ [35,36], for each solution measurements were triplicated obtaining the average ε.

2.5.2. Catalytic reduction of 4-nitrophenol

A fresh aqueous 4-nitrophenol concentrated solution (0.01 M) was prepared by dissolving 0.1391 g of 4-nitrophenol in distilled water in a 100 mL volumetric flask. For each test, 500 μL of a fresh solution ($2.0{\cdot}10^{-4}$ M) was withdrawn from the initial 4-NP concentrated solution and diluted in a 25 mL volumetric flask. Then, the reducing agent dissolved in distilled water (25 mL of a $9.0{\bullet}10^{-3}$ M of $NaBH_4$), and the 4-NP solution was mixed in a beaker. Subsequently 2.5 mL of this solution containing the analyte and the reducing agent was transferred in a cuvette, kept under stirring, containing 0.4 mg of catalyst. The cuvette was inserted into the instrument equipped with integrated stirring and temperature control. An acquisition every 30 s was programmed to evaluate the decrease in the concentration of 4-nitrophenol as a function of time. The analysis was conducted, setting the temperature at 25 °C with stirring at 500 rpm to guarantee the homogenization of the catalysts in the solution. The catalytic tests were performed three times for each fresh material following the same procedure.

The experiments involving changes in the solution pHs were conducted using a round-bottom flask equipped with a glass electrode immersed in the solution to monitor pH over time. Fresh solutions of 4-NP and $NaBH_4$ were diluted with distilled water and adjusted using two solutions of 0.1 M NaOH and 0.1 M HCl to achieve the desired pH value for the reactions. The catalyst amount and reagent concentrations remained consistent with the previously reported values. The solution was stirred at 500 rpm and maintained at a controlled temperature of 25 °C to replicate standard reaction conditions. Every 30 s, a 200 μL aliquot of the solution was withdrawn, diluted with 2.5 mL of distilled water in a quartz cuvette, and analyzed using a UV–visible spectrometer to record absorption spectra. In acidic conditions, the nitrophenolate anion was not formed, resulting in the absence of a strong absorption peak. Therefore, the withdrawn aliquot was diluted with 2.5 mL of 0.01 M NaOH to facilitate the formation of chromophoric species.

3. Results and discussion

The Grzeschik's model suggests an improvement of 4-NP reduction when conducted in acid conditions due to the increase of sodium borohydride hydrolysis rate. Importantly, in this work, we demonstrate an extension of this model for the hybrid catalysts where the medium's acidity is induced from charge surface modification of the polymeric phase during the reaction. To this purpose, polymeric cryogels with different acidity were prepared as support to obtain catalytically active hybrid systems based on gold and palladium nanoparticles. The as-prepared catalysts were tested in the 4-nitrophenol reduction, and the effect of charge surface and solution pH was deeply investigated to elucidate the reaction mechanism involved.

3.1. Cryogels characterization

Bare polymeric cryogels were synthesized via the free-radical cryo-copolymerization method in water at temperatures below its freezing point (Fig. 1). The shaped and interconnected pore structure, due to the porogen role of the ice crystals, was formed during the freezing phase. The thawing generates pores with forms and dimensions depending on the operational parameters used [21]. The high absorption capacity and the possibility to tune the morphology and chemical nature of the functional groups present in the polymeric structure have made these materials suitable supports for immobilizing metal nanoparticles to prepare catalytically active hybrid systems.

The structure of synthesized cryogels has been confirmed by means of ATR-IR spectroscopy. The IR spectra reported in Figure S1 showed the presence of typical acrylic C═O stretching in the range 1750–1650 cm^{-1}. In the same region, the co-presence of two different peaks has been observed: the first at higher wavenumber assigned to carboxylic stretching of acrylic monomers and the second related to the amidic moieties of crosslinked units. Around 1250 cm^{-1}, all samples present the C–O stretching and the absence of a typical peak attributed to the C–C double bond that confirms the success of the polymerization step. Furthermore, the peaks at 3500 cm^{-1} for the *p*-AEMA can be attributed to the N–H stretching (primary amine), and the broad peak at 3300 cm^{-1} is assigned to the O–H stretching of *p*-HEMA (alcohol group) and *p*-MAA (acid group).

To investigate the thermal stability of the synthesized cryogels, thermogravimetric analyses were carried out (Fig. 2). The thermograms were recorded under a nitrogen atmosphere in the 25–800 °C temperature range to evaluate the degradation profile. All samples showed a weight loss at temperatures around 100 °C due to the evaporation of residual water and organic solvent blocked into the polymeric network. In agreement with the literature, the thermal profile of *p*-MAA showed three degradation steps: the first around 240 °C derived from the decarboxylation of the carbonyl groups; the second main step around 430 °C and a third signal (after 650 °C) related to the thermal decomposition of the polymeric backbone [37]. The *p*-AEMA sample displayed three distinct degradation stages at temperatures of 260, 320, and 450 °C, respectively. At lower temperatures, the cleavage of ester linkages resulted in the generation of tertiary amines and alcohols released as gases, and simultaneously, anhydride-type structures were formed in the residual mass. As the temperature increased, a series of unzipping reactions occurred along the polymeric chain, contributing to the overall degradation process [38,39]. Instead, *p*-HEMA cryogel exhibits the absence of well-defined degradation steps, attributed to the concurrent

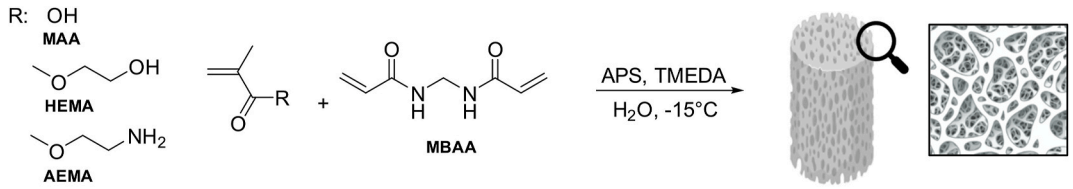

Fig. 1. Schematic representation of cryo-polymerization reaction.

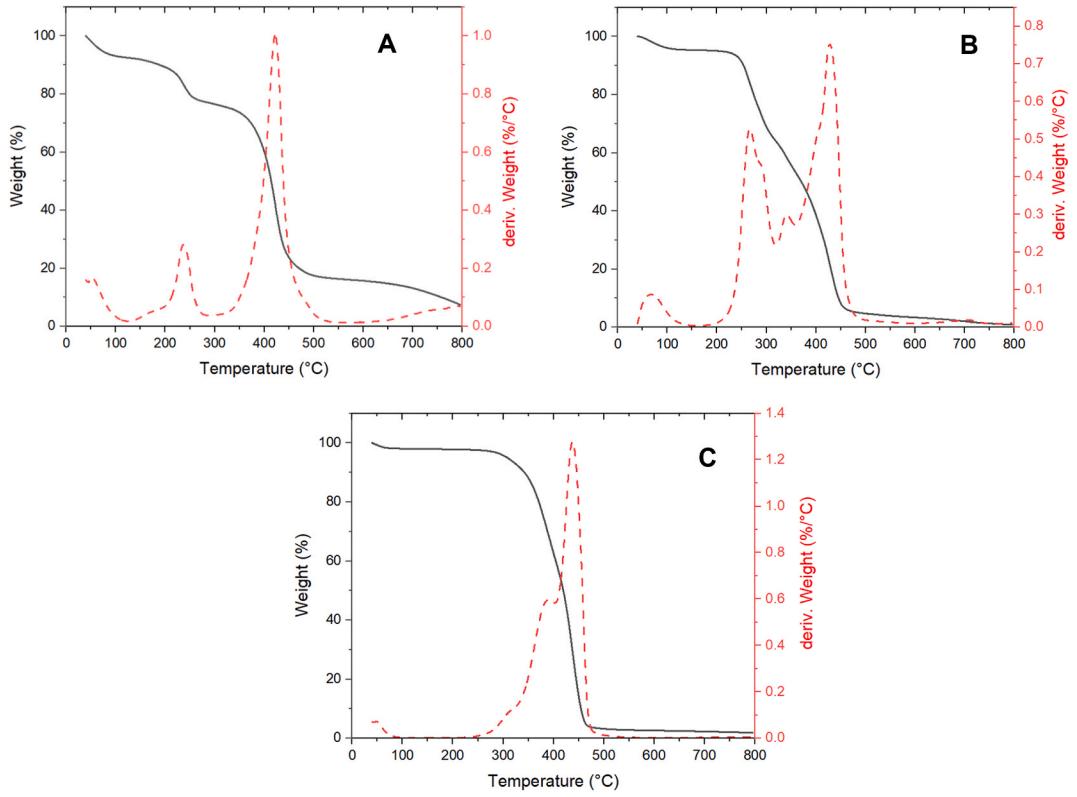

Fig. 2. Thermogravimetric analysis (TGA) of bare cryogels: (A) *p*-MAA,(B) *p*-AEMA, (C) *p*-HEMA.

occurrence of dehydration, chain scission, and depolymerization reactions with a main weight loss in the range of 350–450 °C [40,41]. The main degradation temperature and the related residues for each sample were reported in Table 1.

The morphology of the cryogels was investigated by Scanning Electron Microscopy (SEM); the images reported in Fig. 3 highlighted an interconnected polymeric network for each sample. The prepared bare cryogels showed a peculiar open-pore structure derived from the preparation method and a homogeneous macroporosity. Despite the chemical nature of the cryogel represented a limit to evaluate the porosity of the system with classical methods such as BET or high-pressure mercury porosimetric analysis [42], to have a relative estimation of average pore area ratio, circular equivalent diameter of the porous as well as the porous diameter distribution Phenom Porometric 1.1.2.0 software was employed (Figure S2, Table 1). The porosity values highlighted the absence of significant differences for each sample, confirming the preparation method's validity. As expected, the swelling test results reported in Figure S3 (Table S1) showed high values of swelling for all samples due to the combination of cryogel microporosity structure with the strong hydrophilicity of the functional groups present in the polymer network.

3.2. Preparation and characterization of hybrid metal-polymer nanocatalysts

Polymeric cryogels synthesized in this study were used as platforms for depositing Au and Pd metal nanoparticles through an *in-situ* approach. The method involved initial impregnation of the polymeric matrix with metal precursors ($HAuCl_4$ or K_2PdCl_6) through wet-impregnation, followed by reduction using a fresh solution of $NaBH_4$. The nominal metal loading on the polymer was approximately 1 wt%, and the complete deposition was verified by MP-AES spectroscopy, with

Table 1
Average pore area ratio and circular equivalent diameter of the porous for the bare cryogels.

Sample	T_d (°C)[a]	Residue (%)	Average Pore Area Ratio (%)	The Circular Equivalent Diameter of the Porous (μm)
***p*-MAA**	420	7.5	51	29
***p*-AEMA**	430	0.9	44	25
***p*-HEMA**	440	1.8	47	25

[a] Evaluated by the curve derivate.

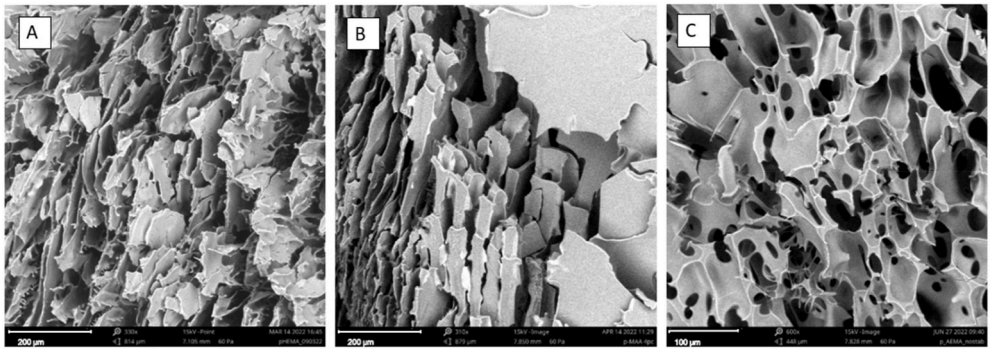

Fig. 3. SEM images of bare cryogels: (A) *p*-HEMA, (B) *p*-MAA, (C) *p*-AEMA.

a negligible amount of unabsorbed metal in the solution. Cryogel swelling enhanced the impregnation process, leading to better absorption and distribution of the nanoparticles on the polymer sponge. Additionally, a shift in colour was noted in the hybrid materials following the reduction process, indicating the formation of nanoparticles within the polymeric matrix [43,44]. Specifically, in the case of gold nanoparticles, this phenomenon can serve as a reliable indicator of the nanoparticles' real size. Within the prepared gold-based system, the presence of a red coloration suggests a nanoparticle diameter ranging between 3 and 5 nm [45]. Characterization of the as-prepared materials involved investigating the metal species' nature, morphology, and thermal properties.

Infrared spectroscopy after impregnation and reduction displayed minor changes, validating the preparation method, and no distinctive peaks from metallic species were observed due to the low metal loading. Combining ATR-IR spectroscopy results with SEM images demonstrated that the impregnation and chemical reduction processes did not alter the cryogel's morphology (Figures S4-5).

To evaluate surface exposure and the oxidation state of the metal for the species deposited onto polymeric cryogel, XPS analysis was carried out (Table 2). The XPS spectra related to Au and Pd for each support employed are reported in Fig. 4 a-b. Regarding gold-based materials, the XPS spectra showed the presence of Au nanoparticles in the metallic state (Au^0). The peaks are composed of spin-orbit doublets (Au $4f_{7/2}$, and Au $4f_{5/2}$). They have characteristic binding energy peaks at 83.8 and 87.5 eV for Au $4f_{7/2}$ and $4f_{5/2}$ electrons, respectively, characteristic of the presence of Au^0 [45,46].

The sample pAEMA_Au showed a significant shift towards lower binding energy due to the presence of amino groups characterized by an electron-donor nature that can modify the surface charge of gold nanoparticles forming $Au^{\delta-}$ species (83.3 eV) [47,48]. The deconvolution analysis carried out on XPS spectra exhibited the presence of Au^0 for each sample, and for the sample pAEMA_Au, the co-presence of Au^0 and $Au^{\delta-}$.

In the case of Pd-based hybrid nanomaterials, peaks at 335.3 and 337.1 eV related to Pd $3d_{5/2}$ and Pd $3d_{3/2}$ were observed [49,50].

Table 2
XPS values (BE, metal surface percentage and Metal/C surface atomic ratio) for each hybrid material.

Sample	BE (eV)[a]	% Metal on Surface	Surface Atomic Ratio M/C	Oxidation state (%)
pHEMA_Au	84.0	0.2	0.003	Au(0)100
pHEMA_Pd	335.0	0.2	0.003	Pd(0) 68 Pd(II) 32
pMAA_Au	84.0	0.4	0.005	Au(0)100
pMAA_Pd	335.1	0.3	0.004	Pd(0) 100
pAEMA_Au	83.3	0.1	0.0003	$Au(0)/Au^{-\delta}$ 100
pAEMA_Pd	335.1	0.5	0.008	Pd(0) 100

[a] Au $4f_{7/2}$ or Pd $3f_{5/2}$ signals.

Despite the broad signals suggesting the co-presence of Pd^{+2} and Pd^0 species, the deconvoluted spectra highlighted both species only in the case of pHEMA_Pd sample (68 % Pd(II) and 32 % Pd(0)). The presence of PdO could be derived from several factors such as the microenvironment around the metal nanoparticles and/or the presence of moisture in the samples that can promote the surface passivation of the nanoparticles [51,52]. Moreover, the amount of metal on the polymer surface is under the nominal amount of metal loaded on the support. This result can be attributed either to the topology of the metal nanoparticles inside the polymer network, where they are placed around and/or inside the pores of the cryogel and therefore hidden during the XPS analysis, justifying the results obtained or the presence of large Pd nanoparticles.

3.3. Catalytic tests

After being ground, the as-prepared materials underwent testing in a batch reactor setup using the reduction of 4-nitrophenol to assess their catalytic performances and investigate the reaction mechanism. Before starting with the catalytic tests of the hybrid materials, a preliminary analysis was conducted to explore each bare cryogel's adsorption capability for 4-nitrophenol. Despite the slight adsorption observed (Figure S6), particularly for the pAEMA sample, the values obtained were negligible compared to the catalytic results achieved in a significantly shorter reaction time (4.5 min). The kinetic data, including the apparent kinetic constant (k_{app}) and percentage conversion, are presented in Table 3. The comparison of results takes into account the type of polymeric support used and the nature of the metal (Figures S7-8).

The catalytic activity observed in the *p*-MAA samples characterized by the presence of acid moieties demonstrated the most effective structural properties, as indicated by a higher apparent kinetic constant. This finding aligns with Grzeschik's model, where the reduction of 4-nitrophenol strongly depends on the dissociation of $NaBH_4$. Specifically, in acidic solutions, the hydrolysis rate of borohydride ions increases, leading to an elevated production of hydrogen capable of entering the catalytic cycle and consequently enhancing catalytic activity (Fig. 5). In our case, the bulk polymeric materials could contribute to the reaction by a pH change inducing a variation of their surface net charge, depending on the dissociation of functional groups on the polymer sponges.

Despite several issues related to TEM analysis on superabsorbent hydrophilic cryogels, the sample, which has exhibited the best catalytic performance (*p*-MAA_Pd), was further characterized by TEM microscopy to evaluate the size of nanoparticles and their topology (Fig. 6) [53,54]. The images highlighted the presence of spherical nanoparticles with dimensions of 2.3 ± 0.6 nm. In addition, a good dispersion of active phase can be observed confirming the validity of the preparation method.

To further investigate this behaviour related to the correlation between pH and catalytic activity, Electrodynamic Light Scattering (ELS) titration measurements as a function of pH were carried out to evaluate

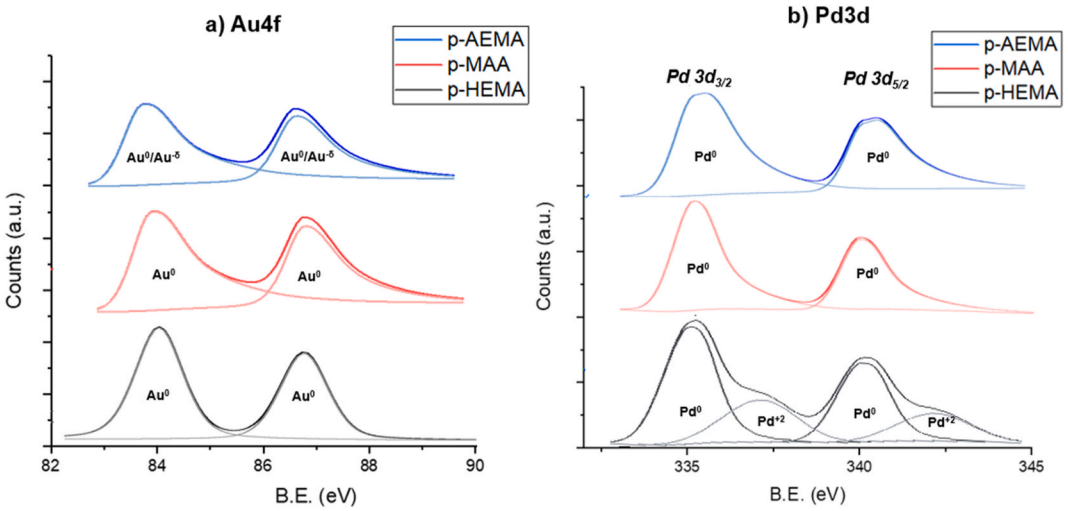

Fig. 4. XPS spectra for the Au-based (a) and Pd-based (b) hybrid materials.

Table 3
XPS data, k_{app} (min^{-1}), and X% of the Au- and Pd-based hybrid nano-catalysts for 4-nitrophenol reduction carried out using 25 mL of 4–NP ($2{\cdot}10^{-4}$ M), 25 mL of $NaBH_4$ ($9{\cdot}10^{-3}$ M), 4 mg of hybrid catalys at 25 °C and 500 rpm.

Sample	k_{app} (min^{-1})[a]	X%[a]	% Metal on Surface
pHEMA_Au	$0.02 \pm 1.4{\cdot}10^{-3}$	7 ± 3	0.2
pHEMA_Pd	$0.53 \pm 6.8{\cdot}10^{-2}$	91 ± 2	0.2
pMAA_Au	$0.30 \pm 8.8{\cdot}10^{-2}$	75 ± 3	0.4
pMAA_Pd	$1.10 \pm 6.1{\cdot}10^{-2}$	99 ± 1	0.3
pAEMA_Au	$0.28 \pm 7.2{\cdot}10^{-2}$	75 ± 3	0.1
pAEMA_Pd	$0.55 \pm 6.6{\cdot}10^{-2}$	93 ± 2	0.5

The results reported are referred to a defined reaction time (4.5 min) to better compare the catalytic activity.
Au $4f_{7/2}$ or Pd $3f_{5/2}$ signals.

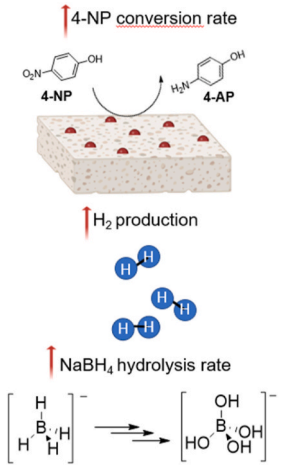

Fig. 5. Schematic reaction mechanism proposed by Grzeschik.

the surface charge at the reaction pH and therefore to measure the surface charge of the organic phase (Fig. 7), [55,56]. Before the analysis, the pH reached during the reaction was measured, and the value detected was 8.4. By analysing the bare cryogels in the pH range of 5–9, it's possible to observe different behaviour for each matrix. The *p*-HEMA characterized from hydroxyl groups exhibited a low zeta potential in the range studied with an isoelectric point (IEP) at pH = 6.6, confirming the absence of surface ionic forms. Instead, *p*-AEMA (bearing amino groups) highlighted an IEP at pH = 8.3 with a low positive charge until IEP value reasonably derived from amine protonation in the acid media. Finally, the *p*-MAA showed a significant surface charge after the IEP (pH = 5.7) and the negative zeta potential at the reaction pH can be ascribed to the presence of deprotonated form of the acrylic acid. In this contest, we can assume that the protons derived from acid dissociation are present in the microenvironment where the metal nanoparticles are located and therefore change the microenvironment pH towards an acid field.

To confirm the results, measurements in the pH range of 6–9 as a function of time was carried out by taking in contact 4 mg of bare cryogels with 50 mL of water and measuring the pH values every 5 min. The experiment was conducted to observe the possible alteration of the pH environment derived from the dissociation of functional groups on the polymer surface.

The results presented in the Supplementary Information (Figure S9) for each cryogel highlight that the pH values changed during the experiments within the pH range of 6–9. This variation is attributed to the contribution of functional groups on the polymeric matrix, influencing the solution's pH. With a reaction time of 4.5 min, the system that exhibited the most significant effect within the defined time was the *p*-MAA cryogel, where a noticeable shift from 7.8 to 6.6 in pH value was observed in the measurements conducted at pH 8. In agreement with the ELS analysis, this behaviour demonstrates that during the reaction the contribution of the polymer matrix affects and alters the acidity of the microenvironment around the nanoparticles. Based on the scheme reported in Fig. 5, an increase in solution acidity can lead to an increase in sodium borohydride hydrolysis rate.

To verify this hypothesis, qualitative tests were carried out for the sodium borohydride decomposition in water by measuring the hydrogen bubble evolution reported in the following reaction scheme. The sodium borohydride decomposition in water was evaluated at different pHs, and results are reported in Figure S10. The experiment was conducted by solubilizing the same amount of $NaBH_4$ used in the reaction (8.5 mg) in 25 mL of deionized water at specific pH values.

The trend illustrated in Figure S10 highlighted an increase of hydrolysis rate while the sodium borohydride was dissolved in acid media. On the other hand, as reported in literature, at higher pH the $NaBH_4$ hydrolysis and therefore hydrogen formation, is slower [57,58]. To further confirm the reaction mechanism and demonstrate the application of Grzeschik's model also for such hybrid catalysts, catalytic tests using the best sample (*p*-MAA_Pd) were carried out conducting the 4-NP reduction at different pH values. The kinetic curves and the related values were illustrated and reported in Fig. 8A–S11 and Table 4, respectively.

Plotting the apparent kinetic constants (k_{app}), calculated from the

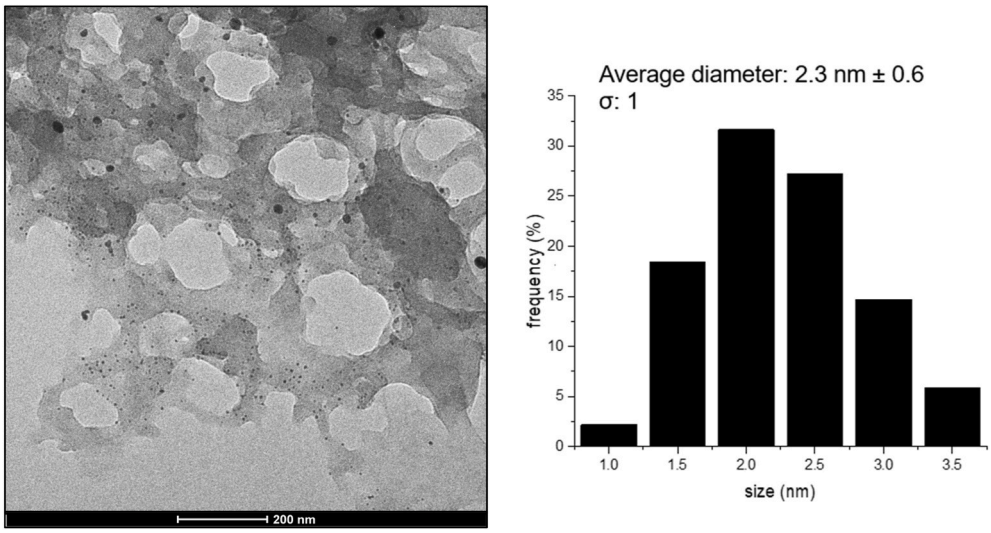

Fig. 6. TEM image and diameter distribution of the sample *p*-MAA_Pd.

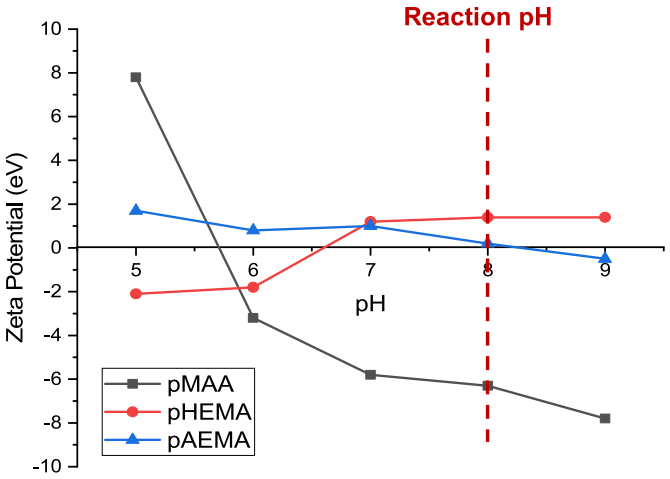

Fig. 7. pH-Zeta potential titration curves for bare cryogels in the pH range 5–9.

Table 4
Kinetic data related to *p*-MAA_Pd for 4-nitrophenol reduction carried out using 25 mL of 4–NP ($2{\cdot}10^{-4}$ M), 25 mL of $NaBH_4$ ($9{\cdot}10^{-3}$ M), 4 mg of hybrid catalys at different reaction pH.

pH	k_{app} (min^{-1})[a]	X%[a]	$NaBH_4$ decompositon time (s)
2	$1.56 \pm 8.8{\cdot}10^{-2}$	99 ± 2	170 ± 15
5	$1.15 \pm 7.2{\cdot}10^{-2}$	99 ± 1	200 ± 20
8	$1.10 \pm 6.1{\cdot}10^{-2}$	99 ± 1	240 ± 20
12	$0.29 \pm 4.5{\cdot}10^{-2}$	37 ± 1	380 ± 20

[a] The results reported are referred to a defined reaction time (4.5 min) in order to better compare the catalytic activity.

kinetic plots, as a function of the pH values reveals a decrease in catalytic performance when the reaction is conducted under basic conditions (pH = 12). Conversely, 4-nitrophenol reduction appears to be more favourable at acidic pH. Furthermore, the results align with the $NaBH_4$ decomposition tests, showing that slower hydrolysis at basic pH corresponds to a decrease in catalytic activity (Fig. 8B). The experimental data, combined with tests on bare cryogels to assess pH changes induced by the dissociation of functional groups on the surface and the Electrophoretic Light Scattering (ELS) curves, suggest the applicability of Grzeschik's model.

In this study, the local induced pH was not directly modified by adding acid/base solutions but by the polymeric matrix, which, under reaction conditions, can deprotonate to form an acidic microenvironment around the nanoparticles, promoting $NaBH_4$ hydrolysis and consequently increasing 4-nitrophenol conversion. The mechanism proposed in Fig. 9 can be considered an extension of the reaction mechanism reported by Grzeschik for cryogel-based hybrid catalysts.

3.4. *Effect of the metal on the catalytic performances*

By analyzing the catalytic results based on the nature of the metal active phase, the observed k_{app} values have highlighted a superior catalytic performance for Pd-based materials compared to the activity of the Au-based hybrid catalysts (refer to Table 3). These results align with existing literature, where multiple papers have documented the heightened affinity of palladium species in forming stable metal-hydrides, consequently enhancing reaction rates during hydrogenation reactions (Fig. 10) [59,60]. Despite the superior catalytic activity of Pd-based catalysts, the data obtained for Au-based materials have showcased good activity compared with those from the literature considering the same reaction time (4.5 min) used in this work [15,61,62]. Furthermore, despite variations in catalytic activity arising from the reactivity of metal nanoparticles, both series of samples underscored the superior catalytic performance of acrylic acid based cryogels. A slight difference can be observed in gold-based materials due to the concurrent electronic effects arising from the amino groups present in the AEMA building block. This effect is evident in the XPS spectra presented in Fig. 3. Despite that, this observation confirms the reaction mechanism proposed in this work.

3.5. *Reusability tests*

To complete the investigation on *p*-MAA_Pd, the most active catalyst, a reusability study was also carried out. These tests were conducted following the same reaction setup described previously. The conversion reached after a defined reaction time of 120 s was used to compare the catalytic activity on the five recycling tests. Despite the conversions slight decreases during the cycles, the catalytic behavior observed has highlighted excellent performances (Fig. 11). Moreover, Microwave Plasma Atomic Emission Spectroscopy (MP-AES) was performed on the reaction solution and revealed that only traces of Pd (below 10 ppb) were detected in the reaction filtrate. This result indicates that no significant leaching has occurred. One of the main reasons for decreased catalytic activity is the slight agglomeration of the Pd nanoparticles during the reaction [63,64].

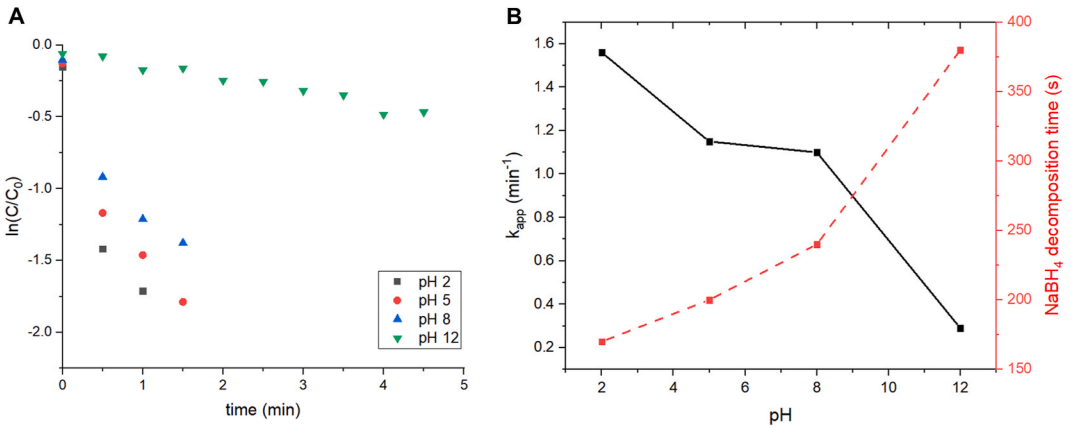

Fig. 8. Pseudo–first−order kinetic plot (A) related to *p*-MAA_Pd for the 4–NP reduction carried out using 25 mL of 4–NP ($2{\cdot}10^{-4}$ M), 25 mL of $NaBH_4$ ($9.0{\cdot}10^{-3}$ M), 4 mg of catalyst at different pH. (B) Correlation between apparent kinetic constant (min^{-1}), reaction pH and $NaBH_4$ decomposition time (s).

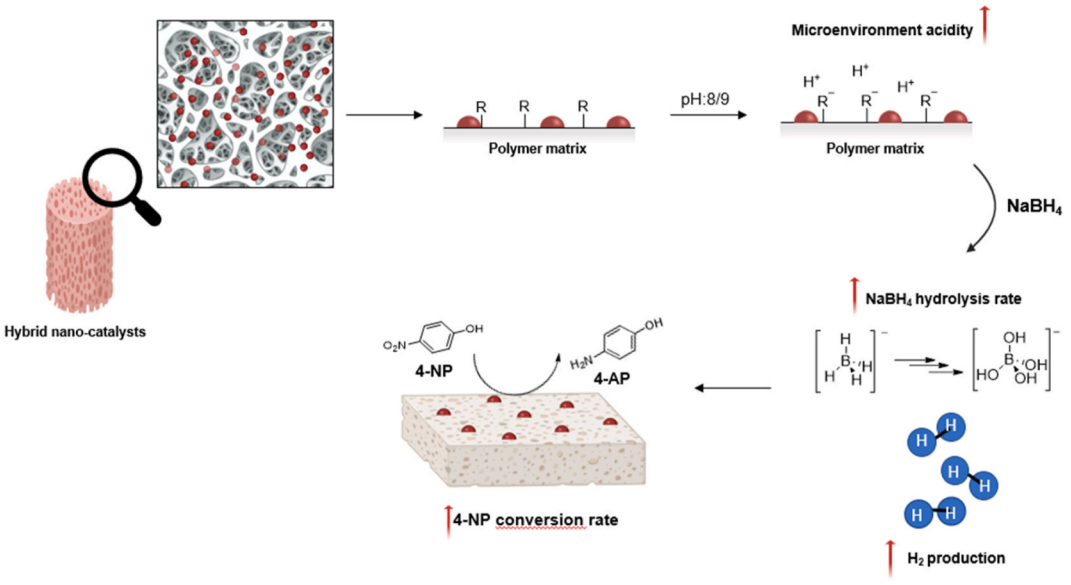

Fig. 9. Proposed reaction mechanism for 4-NP reduction with $NaBH_4$ in the presence of hybrid nano-catalysts.

4. Conclusions

The past decade has witnessed successful testing of various hybrid systems utilizing cryogels as catalytic supports for the conversion of 4-nitrophenol (4-NP) to 4-aminophenol (4-NP), where a pivotal factor influencing the conversion of nitroaromatic compounds is the presence of sodium borohydride.

To this purpose, Grzeschik and colleagues addressed this aspect, shedding light on the influence of solution pH on the dissociation of $NaBH_4$ and its consequential impact on the reduction of 4-NP. In this study, we have conducted a systematic investigation, extending the proposed mechanism to hybrid catalysts by preparing polymeric cryogels characterized by different acid/base properties employed to support the *in-situ* preparation of Au and Pd nanocatalysts.

The catalytic tests have highlighted the strong impact of the acidity nature of the polymeric support in 4-NP reduction, where the poly (acrylic acid)-based catalysts showed a kinetic constant of 1.1 and 0.3 min^{-1} for Pd and Au nanoparticles, respectively, emerging as the best sample of the related series. To further investigate the reaction mechanism, a series of Electrophoretic Light Scattering and time-resolved pH measures were carried out to evaluate the polymeric surface behavior at different pH values, including the reaction pH. A remarkable proof of acid moieties dissociation and, therefore, negative surface charge on the polymer matrix, were reported herein.

To conclude the mechanism analysis, the effect of pH on the sodium borohydride dissociation on the 4-NP reduction was also deeply studied. The outcomes have allowed us to confirm and propose a novel reaction mechanism involving these types of hybrid materials. The effect of polymeric matrix dissociation induces the formation of acid microenvironment around metal nanoparticles, promoting $NaBH_4$ dissociation, and consequently increasing hydrogen formation and 4-NP reaction rate. This finding nicely confirmed and extended the reaction model proposed from Grzeschik. Likewise, the results emphasized the polymer's role in the catalytic mechanism.

Funding

This work has been funded by the European Union (NextGeneration EU) through the MUR-PNRR project SAMOTHRACE – Sicilian Micro-nanoTech Research and Innovation Center (ECS00000022, CUP B63C22000620005).

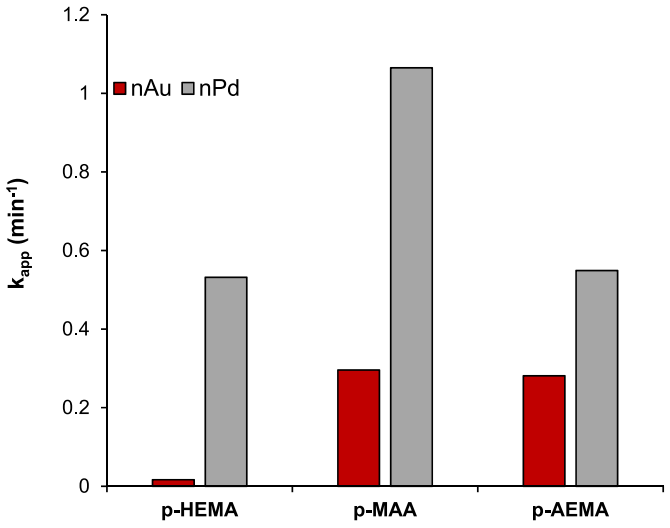

Fig. 10. Catalytic activity of 4-NP reduction, reaction carried out using 25 mL of 4–NP ($2{\cdot}10^{-4}$ M), 25 mL of $NaBH_4$ ($9.0{\cdot}10^{-3}$ M), 4 mg of catalyst at 25 °C and 500 rpm: comparison of the active phase.

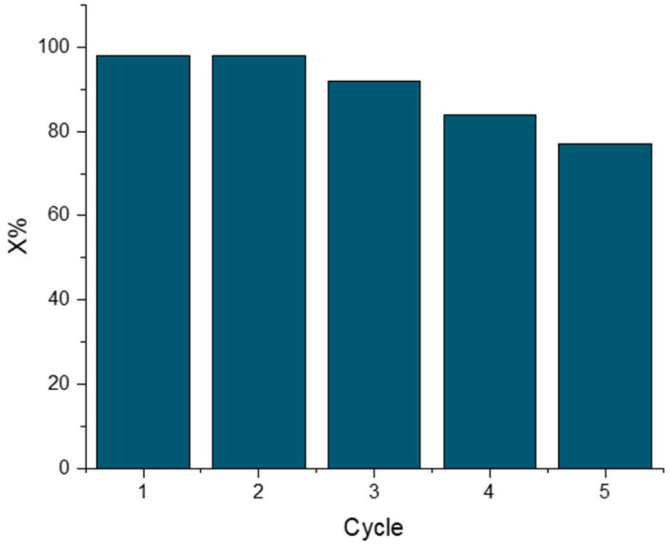

Fig. 11. Plot of conversion per each run of the reusability tests using *p*-MAA_Pd catalyst.

CRediT authorship contribution statement

Stefano Scurti: Writing – review & editing, Writing – original draft, Validation, Supervision, Software, Methodology, Investigation, Formal analysis, Data curation, Conceptualization. **Giuseppe Proietto Salanitri:** Writing – review & editing, Validation, Software, Investigation, Formal analysis, Data curation. **Tommaso Mecca:** Writing – review & editing, Validation, Software, Methodology, Formal analysis, Data curation. **Elena Rodríguez-Aguado:** Writing – review & editing, Software, Resources, Methodology, Formal analysis, Data curation. **Juan Antonio Cecilia:** Writing – review & editing, Software, Methodology, Formal analysis, Data curation. **Giusy Curcuruto:** Writing – review & editing, Software, Resources, Formal analysis, Data curation. **Sabrina Carola Carroccio:** Writing – review & editing, Writing – original draft, Visualization, Supervision, Software, Resources, Methodology, Investigation, Formal analysis, Data curation, Conceptualization. **Daniele Caretti:** Writing – review & editing, Writing – original draft, Visualization, Supervision, Resources, Project administration, Methodology, Investigation, Formal analysis, Data curation, Conceptualization. **Nikolaos Dimitratos:** Writing – review & editing, Visualization, Supervision, Methodology, Conceptualization.

Declaration of competing interest

The authors declare that they have no known competing financial interests or personal relationships that could have appeared to influence the work reported in this paper.

Data availability

Data will be made available on request.

Acknowledgments

The authors want to thank Cristina Del Barone and Pierfrancesco Cerruti for the precious support for the TEM analysis.

Appendix A. Supplementary data

Supplementary data to this article can be found online at https://doi.org/10.1016/j.mtchem.2024.102046.

References

[1] R. Javed, M. Zia, S. Naz, S.O. Aisida, N. ul Ain, Q. Ao, Role of capping agents in the application of nanoparticles in biomedicine and environmental remediation: recent trends and future prospects, J. Nanobiotechnol. 18 (2020) 1–15.
[2] H. He, X. Shen, Z. Nie, Engineering interactions between nanoparticles using polymers, Prog. Polym. Sci. 143 (2023) 101710, https://doi.org/10.1016/j.progpolymsci.2023.101710.
[3] X. Lin, S. Ye, C. Kong, K. Webb, C. Yi, S. Zhang, Q. Zhang, J.T. Fourkas, Z. Nie, Polymeric ligand-mediated regioselective bonding of plasmonic nanoplates and nanospheres, J. Am. Chem. Soc. 142 (2020) 17282–17286, https://doi.org/10.1021/jacs.0c08135.
[4] S. Mourdikoudis, L.M. Liz-Marzán, Oleylamine in nanoparticle synthesis, Chem. Mater. 25 (2013) 1465–1476, https://doi.org/10.1021/cm4000476.
[5] L.M. Rossi, J.L. Fiorio, M.A.S. Garcia, C.P. Ferraz, The role and fate of capping ligands in colloidally prepared metal nanoparticle catalysts, Dalton Trans. 47 (2018) 5889–5915, https://doi.org/10.1039/C7DT04728B.
[6] D. González-Gálvez, P. Nolis, K. Philippot, B. Chaudret, P.W.N.M. van Leeuwen, Phosphine-Stabilized ruthenium nanoparticles: the effect of the nature of the ligand in catalysis, ACS Catal. 2 (2012) 317–321, https://doi.org/10.1021/cs200633k.
[7] D. Li, S. Komarneni, Microwave-assisted polyol process for synthesis of Ni nanoparticles, J. Am. Ceram. Soc. 89 (2006) 1510–1517, https://doi.org/10.1111/j.1551-2916.2006.00925.x.
[8] L. Jin, B. Liu, S. Duay, J. He, Engineering surface ligands of noble metal nanocatalysts in tuning the product selectivity, Catalysts 7 (2017) 44, https://doi.org/10.3390/catal7020044.
[9] A. Villa, D. Wang, D.S. Su, L. Prati, Gold sols as catalysts for glycerol oxidation: the role of stabilizer, ChemCatChem 1 (2009) 510–514.
[10] S. Campisi, D. Ferri, A. Villa, W. Wang, D. Wang, O. Kröcher, L. Prati, Selectivity control in palladium-catalyzed alcohol oxidation through selective blocking of active sites, J. Phys. Chem. C 120 (2016) 14027–14033, https://doi.org/10.1021/acs.jpcc.6b01549.
[11] S.M. Ansar, C.L. Kitchens, Impact of gold nanoparticle stabilizing ligands on the colloidal catalytic reduction of 4-nitrophenol, ACS Catal. 6 (2016) 5553–5560, https://doi.org/10.1021/acscatal.6b00635.
[12] P. Zhang, T.K. Sham, Tuning the electronic behavior of Au nanoparticles with capping molecules, Appl. Phys. Lett. 81 (2002) 736–738, https://doi.org/10.1063/1.1494120.
[13] Y. Zhao, J. Baeza, N.K. Rao, L. Calvo, M. Gilarranz, Y. Li, L. Lefferts, Unsupported PVA-and PVP-stabilized Pd nanoparticles as catalyst for nitrite hydrogenation in aqueous phase, J. Catal. 318 (2014) 162–169.
[14] C. Sanchez, K.J. Shea, S. Kitagawa, Recent progress in hybrid materials science, Chem. Soc. Rev. 40 (2011) 471, https://doi.org/10.1039/c1cs90001c.
[15] D. Berillo, Gold nanoparticles incorporated into cryogel walls for efficient nitrophenol conversion, J. Clean. Prod. 247 (2020) 119089, https://doi.org/10.1016/j.jclepro.2019.119089.
[16] K. Xia, K. Yamaguchi, K. Suzuki, Recent advances in hybrid materials of metal nanoparticles and polyoxometalates, Angew. Chem. Int. Ed. 62 (2023) e202214506.
[17] A.-L. Gu, W.-T. Wang, X.-Y. Cheng, T.-D. Hu, Z.-L. Wu, Non-noble-metal metal–organic-framework-catalyzed carboxylative cyclization of propargylic amines with atmospheric carbon dioxide under ambient conditions, Inorg. Chem. 60 (2021) 13425–13433, https://doi.org/10.1021/acs.inorgchem.1c01776.

[18] S. Kudaibergenov, Physicochemical, complexation and catalytic properties of polyampholyte cryogels, Gels 5 (2019) 8, https://doi.org/10.3390/gels5010008.
[19] S.E. Kudaibergenov, G.I. Dzhardimalieva, Flow-through catalytic reactors based on metal nanoparticles immobilized within porous polymeric gels and surfaces/hollows of polymeric membranes, Polymers 12 (2020) 572, https://doi.org/10.3390/polym12030572.
[20] Y. Xiang, Y. Liu, X. Ma, W. Bai, L. Xu, C. Cao, G. Liu, Modified phenolic resin for the removal and reduction of Au(III) and simultaneously as the nano-Au(0) immobilized carrier for catalysis, React. Funct. Polym. 179 (2022) 105358, https://doi.org/10.1016/j.reactfunctpolym.2022.105358.
[21] A. Baimenov, D.A. Berillo, S.G. Poulopoulos, V.J. Inglezakis, A review of cryogels synthesis, characterization and applications on the removal of heavy metals from aqueous solutions, Adv. Colloid Interface Sci. 276 (2020) 102088, https://doi.org/10.1016/j.cis.2019.102088.
[22] A. Haleem, J.-M. Pan, A. Shah, H. Hussain, W. He, A systematic review on new advancement and assessment of emerging polymeric cryogels for environmental sustainability and energy production, Separ. Purif. Technol. 316 (2023) 123678, https://doi.org/10.1016/j.seppur.2023.123678.
[23] A. Haleem, S.-Q. Chen, M. Ullah, M. Siddiq, W.-D. He, Highly porous cryogels loaded with bimetallic nanoparticles as an efficient antimicrobial agent and catalyst for rapid reduction of water-soluble organic contaminants, J. Environ. Chem. Eng. 9 (2021) 106510, https://doi.org/10.1016/j.jece.2021.106510.
[24] T. Soboleva, X. Zhao, K. Malek, Z. Xie, T. Navessin, S. Holdcroft, On the micro-, meso-, and macroporous structures of polymer electrolyte membrane fuel cell catalyst layers, ACS Appl. Mater. Interfaces 2 (2010) 375–384, https://doi.org/10.1021/am900600y.
[25] J. Ambreen, A. Haleem, A.A. Shah, F. Mushtaq, M. Siddiq, M.A. Bhatti, S.N.U. Shah Bukhari, A.D. Chandio, W.A. Mahdi, S. Alshehri, Facile synthesis and fabrication of NIPAM-based cryogels for environmental remediation, Gels 9 (2023) 64, https://doi.org/10.3390/gels9010064.
[26] N. Sahiner, F. Seven, The use of superporous p(AAc (acrylic acid)) cryogels as support for Co and Ni nanoparticle preparation and as reactor in H2 production from sodium borohydride hydrolysis, Energy 71 (2014) 170–179, https://doi.org/10.1016/j.energy.2014.04.031.
[27] S. Wunder, F. Polzer, Y. Lu, Y. Mei, M. Ballauff, Kinetic analysis of catalytic reduction of 4-nitrophenol by metallic nanoparticles immobilized in spherical polyelectrolyte brushes, J. Phys. Chem. C 114 (2010) 8814–8820, https://doi.org/10.1021/jp101125j.
[28] A. Iben Ayad, D. Luart, A. Ould Dris, E. Guénin, Kinetic analysis of 4-nitrophenol reduction by "water-soluble" palladium nanoparticles, Nanomaterials 10 (2020) 1169, https://doi.org/10.3390/nano10061169.
[29] S. Gu, S. Wunder, Y. Lu, M. Ballauff, R. Fenger, K. Rademann, B. Jaquet, A. Zaccone, Kinetic analysis of the catalytic reduction of 4-nitrophenol by metallic nanoparticles, J. Phys. Chem. C 118 (2014) 18618–18625, https://doi.org/10.1021/jp5060606.
[30] F. Lin, R. Doong, Highly efficient reduction of 4-nitrophenol by heterostructured gold-magnetite nanocatalysts, Appl. Catal. Gen. 486 (2014) 32–41, https://doi.org/10.1016/j.apcata.2014.08.013.
[31] A.V. Churikov, I.M. Gamayunova, K.V. Zapsis, M.A. Churikov, A.V. Ivanishchev, Influence of temperature and alkalinity on the hydrolysis rate of borohydride ions in aqueous solution, Int. J. Hydrogen Energy 37 (2012) 335–344, https://doi.org/10.1016/j.ijhydene.2011.09.066.
[32] R. Grzeschik, D. Schäfer, T. Holtum, S. Küpper, A. Hoffmann, S. Schlücker, On the overlooked critical role of the pH value on the kinetics of the 4-nitrophenol $NaBH_4$-reduction catalyzed by noble-metal nanoparticles (Pt, Pd, and Au), J. Phys. Chem. C 124 (2020) 2939–2944, https://doi.org/10.1021/acs.jpcc.9b07114.
[33] B.M.A. Carvalho, S.L. Da Silva, L.H.M. Da Silva, V.P.R. Minim, M.C.H. Da Silva, L. M. Carvalho, L.A. Minim, Cryogel poly(acrylamide): synthesis, structure and applications, Separ. Purif. Rev. 43 (2014) 241–262, https://doi.org/10.1080/15422119.2013.795902.
[34] T. Mecca, M. Ussia, D. Caretti, F. Cunsolo, S. Dattilo, S. Scurti, V. Privitera, S. C. Carroccio, N-methyl-D-glucamine based cryogels as reusable sponges to enhance heavy metals removal from water, Chem. Eng. J. 399 (2020) 125753, https://doi.org/10.1016/j.cej.2020.125753.
[35] D. Motta, F. Sanchez, K. Alshammari, L.E. Chinchilla, G.A. Botton, D. Morgan, T. Tabanelli, A. Villa, C. Hammond, N. Dimitratos, Preformed Au colloidal nanoparticles immobilised on NiO as highly efficient heterogeneous catalysts for reduction of 4-nitrophenol to 4-aminophenol, J. Environ. Chem. Eng. 7 (2019) 103381, https://doi.org/10.1016/j.jece.2019.103381.
[36] A. Rehor, N.E. Botterhuis, J.A. Hubbell, N.a.J.M. Sommerdijk, N. Tirelli, Glucose sensitivity through oxidation responsiveness : an example of cascade-responsive nano-sensors, J. Mater. Chem. 15 (2005) 4006–4009, https://doi.org/10.1039/b510998a.
[37] K. Şarkaya, A. Allı, Synthesis and characterization of cryogels of p(HEMA-N-vinylformamide) and p(HEMA-N-Vinylpyrrolidone) for chemical release behaviour, J. Porous Mater. 28 (2021) 853–865, https://doi.org/10.1007/s10934-021-01037-9.
[38] A.R.P. Figueiredo, A.G.P.R. Figueiredo, N.H.C.S. Silva, A. Barros-Timmons, A. Almeida, A.J.D. Silvestre, C.S.R. Freire, Antimicrobial bacterial cellulose nanocomposites prepared by in situ polymerization of 2-aminoethyl methacrylate, Carbohydr. Polym. 123 (2015) 443–453, https://doi.org/10.1016/j.carbpol.2015.01.063.
[39] J. Cervantes-Uc, J. Cauich-Rodriguez, W. Herrera-Kao, H. Vazquez-Torres, A. Marcos-Fernandez, Thermal degradation behavior of polymethacrylates containing amine side groups, Polym. Degrad. Stabil. 93 (2008) 1891–1900.
[40] N. Sahiner, S. Demirci, Conducting semi-interpenetrating polymeric composites via the preparation of poly(aniline), poly(thiophene), and poly(pyrrole) polymers within superporous poly(acrylic acid) cryogels, React. Funct. Polym. 105 (2016) 60–65, https://doi.org/10.1016/j.reactfunctpolym.2016.05.017.
[41] K. Demirelli, M. Coşkun, E. Kaya, A detailed study of thermal degradation of poly (2-hydroxyethyl methacrylate), Polym. Degrad. Stabil. 72 (2001) 75–80, https://doi.org/10.1016/S0141-3910(00)00204-4.
[42] A. Kumar, Supermacroporous Cryogels: Biomedical and Biotechnological Applications, CRC Press, 2016.
[43] P.N. Njoki, I.-I.S. Lim, D. Mott, H.-Y. Park, B. Khan, S. Mishra, R. Sujakumar, J. Luo, C.-J. Zhong, Size correlation of optical and spectroscopic properties for gold nanoparticles, J. Phys. Chem. C 111 (2007) 14664–14669.
[44] X. Huang, M.A. El-Sayed, Gold nanoparticles: optical properties and implementations in cancer diagnosis and photothermal therapy, J. Adv. Res. 1 (2010) 13–28.
[45] S. Scurti, E. Monti, E. Rodríguez-Aguado, D. Caretti, J.A. Cecilia, N. Dimitratos, Effect of polyvinyl alcohol ligands on supported gold nano-catalysts: morphological and kinetics studies, Nanomaterials 11 (2021) 879, https://doi.org/10.3390/nano11040879.
[46] S. Scurti, A. Allegri, F. Liuzzi, E. Rodríguez-Aguado, J.A. Cecilia, S. Albonetti, D. Caretti, N. Dimitratos, Temperature-dependent activity of gold nanocatalysts supported on activated carbon in redox catalytic reactions: 5-hydroxymethylfurfural oxidation and 4-nitrophenol reduction comparison, Catalysts 12 (2022) 323, https://doi.org/10.3390/catal12030323.
[47] H. Goodman, L. Mei, T.L. Gianetti, Molecular orbital insights of transition metal-stabilized carbocations, Front. Chem. 7 (2019) 365, https://doi.org/10.3389/fchem.2019.00365.
[48] R.P. Herrera, M.C. Gimeno, Main avenues in gold coordination chemistry, Chem. Rev. 121 (2021) 8311–8363, https://doi.org/10.1021/acs.chemrev.0c00930.
[49] S. Hafeez, F. Sanchez, S.M. Al-Salem, A. Villa, G. Manos, N. Dimitratos, A. Constantinou, Decomposition of additive-free formic acid using a Pd/C catalyst in flow: experimental and CFD modelling studies, Catalysts 11 (2021) 341, https://doi.org/10.3390/catal11030341.
[50] O.A. Ojelade, S.F. Zaman, M.A. Daous, A.A. Al-Zahrani, A.S. Malik, H. Driss, G. Shterk, J. Gascon, Optimizing Pd:Zn molar ratio in PdZn/CeO2 for CO2 hydrogenation to methanol, Appl. Catal. Gen. 584 (2019) 117185, https://doi.org/10.1016/j.apcata.2019.117185.
[51] J. Rogal, K. Reuter, M. Scheffler, Thermodynamic stability of PdO surfaces, Phys. Rev. B 69 (2004) 075421.
[52] H.H. Kan, J.F. Weaver, Mechanism of PdO thin film formation during the oxidation of Pd (1 1 1), Surf. Sci. 603 (2009) 2671–2682.
[53] M.R. Libera, R.F. Egerton, Advances in the transmission electron microscopy of polymers, Polym. Rev. 50 (2010) 321–339.
[54] Y. Lin, M. Zhou, X. Tai, H. Li, X. Han, J. Yu, Analytical transmission electron microscopy for emerging advanced materials, Matter 4 (2021) 2309–2339.
[55] Z. Yuan, J. Wang, Y. Wang, Q. Liu, Y. Zhong, Y. Wang, L. Li, S.F. Lincoln, X. Guo, Preparation of a poly(acrylic acid) based hydrogel with fast adsorption rate and high adsorption capacity for the removal of cationic dyes, RSC Adv. 9 (2019) 21075–21085, https://doi.org/10.1039/C9RA03077H.
[56] C. Zagni, S. Dattilo, T. Mecca, C. Gugliuzzo, A.A. Scamporrino, V. Privitera, R. Puglisi, S. Carola Carroccio, Single and dual polymeric sponges for emerging pollutants removal, Eur. Polym. J. 179 (2022) 111556, https://doi.org/10.1016/j.eurpolymj.2022.111556.
[57] H.N. Abdelhamid, A review on hydrogen generation from the hydrolysis of sodium borohydride, Int. J. Hydrogen Energy 46 (2021) 726–765, https://doi.org/10.1016/j.ijhydene.2020.09.186.
[58] L. Shi, Q. Tang, B. Yang, B. Li, C. Yang, Y. Jin, Acid-accelerated hydrolysis of NaBH4: a gas-generation reaction for diverse gas pressure biosensing, Microchim. Acta 190 (2023) 69, https://doi.org/10.1007/s00604-023-05655-9.
[59] L.J. Bannenberg, B. Boshuizen, F.A. Ardy Nugroho, H. Schreuders, Hydrogenation kinetics of metal hydride catalytic layers, ACS Appl. Mater. Interfaces 13 (2021) 52530–52541, https://doi.org/10.1021/acsami.1c13240.
[60] M.W. Tew, M. Janousch, T. Huthwelker, J.A. van Bokhoven, The roles of carbide and hydride in oxide-supported palladium nanoparticles for alkyne hydrogenation, J. Catal. 283 (2011) 45–54, https://doi.org/10.1016/j.jcat.2011.06.025.
[61] W. Shen, Y. Qu, X. Pei, S. Li, S. You, J. Wang, Z. Zhang, J. Zhou, Catalytic reduction of 4-nitrophenol using gold nanoparticles biosynthesized by cell-free extracts of Aspergillus sp. WL-Au, J. Hazard Mater. 321 (2017) 299–306, https://doi.org/10.1016/j.jhazmat.2016.07.051.
[62] P. Zhao, X. Feng, D. Huang, G. Yang, D. Astruc, Basic concepts and recent advances in nitrophenol reduction by gold- and other transition metal nanoparticles, Coord. Chem. Rev. 287 (2015) 114–136, https://doi.org/10.1016/j.ccr.2015.01.002.
[63] Z. Dong, X. Le, Y. Liu, C. Dong, J. Ma, Metal organic framework derived magnetic porous carbon composite supported gold and palladium nanoparticles as highly efficient and recyclable catalysts for reduction of 4-nitrophenol and hydrodechlorination of 4-chlorophenol, J. Mater. Chem. A 2 (2014) 18775–18785.
[64] A. Kumbhar, Palladium catalyst supported on zeolite for cross-coupling reactions: an overview of recent advances, Top. Curr. Chem. 375 (2017) 2, https://doi.org/10.1007/s41061-016-0084-5.